Hindawi
Journal of Engineering
Volume 2023, Article ID 5572523, 10 pages
https://doi.org/10.1155/2023/5572523

Research Article

Comparative Analysis of Edge Soiling Resilience: Full-Cell vs. Half-Cell Photovoltaic Modules in Different Mounting Orientations

Jicheng Zhou,[1,2] Li Yu ,[2] Ayipaiyili Yuetikuer,[2] Linzhao Hao,[1] and Bingchun Jiang [1]

[1]*Guangdong University of Science and Technology, Dongguan 523083, China*
[2]*School of Energy Science and Engineering, Central South University, Changsha 410083, China*

Correspondence should be addressed to Li Yu; 614365591@qq.com and Bingchun Jiang; jiangbingchun_2008@163.com

Received 11 August 2023; Revised 20 October 2023; Accepted 27 October 2023; Published 2 November 2023

Academic Editor: Assed Naked Haddad

The performance of distributed PV systems is often hindered by edge soiling, mainly due to the challenges associated with centralized cleaning. In recent years, half-cell modules have gained popularity over conventional full-cell modules due to their potential for improved performance. However, limited research has been conducted to compare the effects of edge soiling on full-cell and half-cell modules, particularly in various mounting orientations. Furthermore, there is a scarcity of methods that integrate simulation and experimentation to analyze the characteristics of shaded PV modules. This study aims to optimize module selection and mounting orientation to mitigate the impact of edge soiling. Simulated models and experimental setups were developed for both full-cell and half-cell modules in both landscape and portrait orientations. The results reveal that the degree of shading correlates with the ratio of shaded substrings within a module. In addition, module performance can be significantly enhanced by altering the mounting orientation. Specifically, the findings demonstrate that half-cell modules outperform full-cell modules when mounted in the portrait orientation. However, in the landscape orientation, the advantage of half-cell modules diminishes. Remarkably, the choice of mounting orientation is found to be contingent on the severity of edge soiling for half-cell modules. This work significantly contributes to the understanding of shading effects in PV systems and offers practical guidance for optimizing distributed PV systems against edge soiling.

1. Introduction

The use of distributed energy resources is gaining popularity as a complementary and alternative solution to conventional central power stations [1, 2]. With advancements in photovoltaic (PV) technology, distributed PV systems for residential buildings have become a prevailing trend, offering greater efficiency (>20%) and various advantages, such as easy local accommodation, minimal impact on the power grid, and better utilization of ambient resources [3].

One of the primary considerations when establishing a distributed PV system is the impact of shade on PV modules [4]. Partial shading caused by chimneys, trees, or accumulated dust can significantly impede PV output performance [5, 6]. Specifically, "soiling" means contamination of module surfaces, and thus dust accumulation near the edge of the PV modules is called "edge soiling." Edge soiling is influenced by many factors, such as PV module tilt angle, dust compositions and particle size distributions, wind speeds, and relative humidity [5, 7–9]. In distributed PV systems, edge soiling, often resulting from the lack of centralized cleaning, poses a considerable challenge. The presence of edge soiling leads to inhomogeneous shading and a sharp decline in PV module performance [10].

Shaded cells within a module become reverse biased, acting as loads rather than electrical generators. This generates excessive heat, potentially causing irreversible damage to the cells or modules [11, 12]. For a PV array, edge soiling causes inhomogeneous solar irradiance, leading to an electrical mismatch between the components, and aggravating the power output [13–15]. Bypass diodes have been introduced to mitigate the current mismatch between series

[16]. However, they also bring multiple electrical power output peaks in the power characteristic curves. Multiple local peaks increase the difficulty and complexity of system design to track the global peaks [17, 18].

New PV modules such as half-cell modules emerging within a few years begin to occupy the market. Half-cell modules are believed to have less electrical resistance and light losses compared with full-cell modules, resulting in improved module efficiencies [19, 20]. Half-cell modules also exhibit different shading responses [21]. However, research on the effects of edge soiling on both full-cell and half-cell modules simultaneously have been limited. In addition, the fundamental characterization of PV modules under edge soiling is lacking, leading to ambiguous analyses of bypass diode working principles and other electrical parameters. Moreover, the combination of simulation and experimentation to study the comparison between full-/half-cell modules under edge soiling remains scarce, hindering practical applications.

In this work, we optimize the practical mounting orientations by analyzing the edge soiling effects on the full-/half-cell modules. As shown in Figure 1, four typical soiling patterns are designed. First, we demonstrate the method to create the soiling patterns in Simulink to theoretically predict the module characteristics under edge soiling models. With simulation results, corresponding experiments are conducted under the standard testing condition (STC) with available commercial PV modules. According to contrasting performance of full-cell and half-cell modules under different shading conditions, it can be hypothesized that the choice of module type and mounting orientation should be tailored to the specific shading characteristics of the installation site to maximize energy generation. This work offers an important opportunity to advance the understanding of the essence of edge soiling effects and different responses of full-cell and half-cell modules. It also provides insightful models to investigate PV modules and practical guidance for selecting suitable PV module types for distributed PV systems.

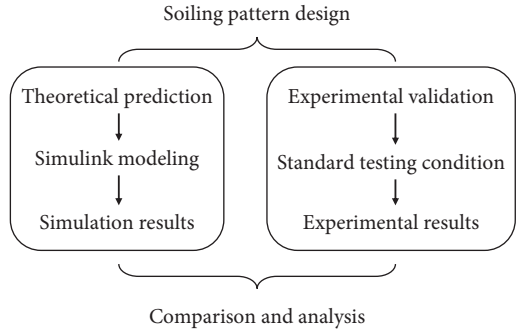

Figure 1: Flowchart of the contents.

2. Methodology

In our study, we investigated two types of commercial PV modules: the full-cell module and the half-cell module. The full-cell module consists of 60 solar cells connected in series (Figure 2(a)). To prevent hotspots and significant power loss, these cells are divided into three substrings, each equipped with a bypass diode (Figure 2(a)). In contrast, the half-cell module contains 120 halved cells, with 60 cells arranged in series for each part (Figure 2(b)). The two parts are then connected in parallel to the terminals, which are situated along the middle and parallel to the width of the module. This interconnection arrangement results in six substrings formed by three bypass diodes (Figure 2(b)). By using these interconnection designs, both module types aim to optimize performance and reduce the impact of shading on PV output.

Figures 2(c) and 2(d) illustrate the characteristic curves of both modules under the standard testing condition. Table 1 presents the comprehensive electrical parameters employed for the simulations. Notably, the full-cell module exhibits an efficiency of 19.2%, while the half-cell module achieves a slightly higher efficiency of 20.3%. These results suggest that both modules perform comparably under unshaded conditions.

A bypass diode is typically connected in parallel to a solar cell or substring, albeit with reversed polarity. During normal operation, each solar cell becomes forward biased, rendering the bypass diode effectively reverse biased, thus behaving as an open circuit. Nevertheless, when a solar cell experiences reverse bias due to a disparity in short-circuit current among multiple series-connected cells, the bypass diode becomes conductive. This conductive state allows the current generated by the unaffected solar cells to flow within the external circuit rather than causing forward bias in each of the unaffected cells. A more comprehensive illustration is shown by Figures 2(e) and 2(f), where the *I-V* curves of the shaded cell, other normal cells and the combined substring are depicted. As a channel for excessive current, the bypass diode avoids power loss and heating by shaded cells.

A PV module can be seen as an interconnection of cells. Before obtaining the module characteristics, we should firstly introduce the mathematical model of a single solar cell. A solar cell is electrically equivalent to a diode with a photocurrent source (I_{ph}), a series resistor (R_s), and a shunt resistor (R_{sh}) [22], which can be expressed as follows:

$$\text{Photocurrent } I_{ph}\text{: } I_{ph} = \left[I_{sc} + k_i \cdot (T - 298)\right] \cdot \frac{G}{1000}, \tag{1}$$

$$\text{Saturation current } I_0\text{: } I_0 = I_{rs} \cdot \left(\frac{T}{T_n}\right)^3 \cdot \exp\left[\frac{q \cdot E_{g0} \cdot \left(1/T_n - 1/T\right)}{n \cdot K}\right],$$

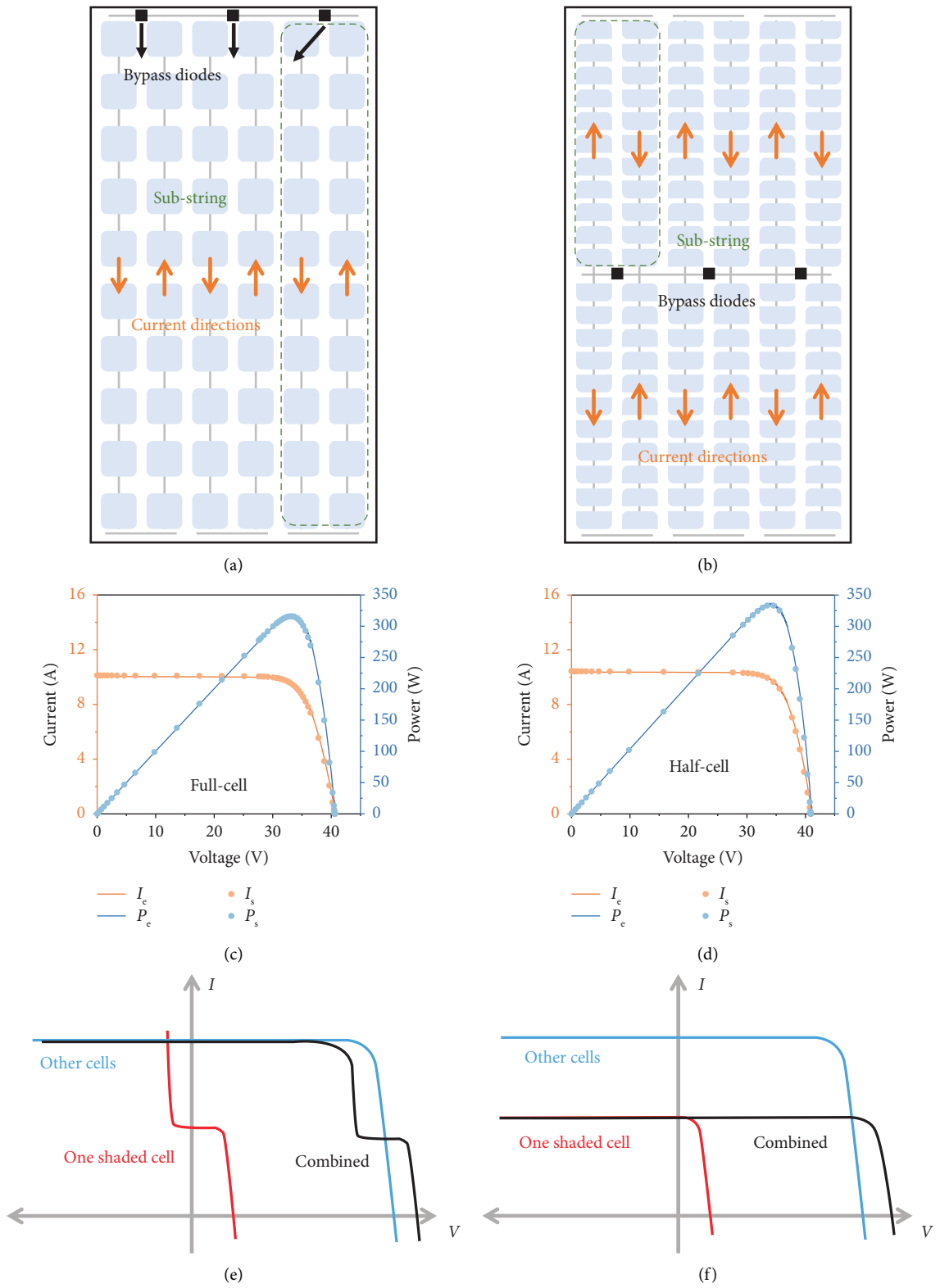

FIGURE 2: Schematics and characteristic curves of the standard 60-full-cell module and 120-half-cell module. (a, b) Schematic views of the full-cell and half-cell modules in portrait mounting orientation, respectively. Each module contains three black dots, which represent the bypass diodes strategically positioned to divide the cells into three (full-cell module) or six (half-cell module) relatively independent substrings, as indicated by the green dotted boxes. The orange arrows indicate the current directions and the polarity of each cell within the modules. (c, d) Characteristic curves of the 60-full-cell module and the 120-half-cell module, respectively. The solid line represents experimental results while the dots represent simulated results. (e, f) The I-V curves of a substring with (e)/without (f) a bypass diode for the shaded cell. All line charts in this paper are edited by Origin.

Table 1: Electrical parameters of commercial PV modules in this work.

Parameters	Notation	Unit	Value	
			Full-cell	Half-cell
Open-circuit voltage	V_{oc}	V	40.72	41.12
Short-circuit current	I_{sc}	A	10.04	10.37
Voltage at MPP	V_{max}	V	33.26	33.99
Current at MPP	I_{max}	A	9.52	9.85
MPP	P_{max}	W	316.75	334.98
Fill factor	FF	%	77.50	78.53

$$\text{Reverse saturation current } I_{rs}\text{: } I_{rs} = \frac{I_{sc}}{\exp\left(q \cdot V_{oc}/n \cdot K \cdot T\right) - 1}, \tag{3}$$

$$\text{Current through shunt resistor } I_{sh}\text{: } I_{sh} = \frac{V + I \cdot R_s}{R_{sh}}, \tag{4}$$

$$\text{Output current } I\text{: } I = I_{ph} - I_0 \cdot \left\{\exp\left[\frac{q \cdot \left(V + I \cdot R_s\right)}{n \cdot K \cdot T}\right] - 1\right\} - I_{sh}, \tag{5}$$

where I_{sc} (A) is the short-circuit current under the STC; k_i (0.0032) is the attenuation coefficient; T (K) is the temperature of the cell; T_n (298 K) is the nominal temperature; G ($W{\cdot}m^{-2}$) is the incident solar irradiance; q ($1.6e-19$°C) is an electron's charge; V_{oc} (V) is the open-circuit voltage; n (1~2) is the diode ideality factor; K ($1.38e10-23\,J{\cdot}K^{-1}$) is Boltzmann's constant; E_{g0} (eV) is the band gap for semiconductors; and V (V) is the output voltage.

The forward biased I–V curve for solar cells uses the one-diode model defined in equation (5) while the reverse-biased I–V curve is simulated by using the Bishop model expressed in the following equation [23]:

$$\begin{aligned} I = I_{ph} - I_0 \cdot \left\{\exp\left[\frac{q \cdot \left(V + I \cdot R_s\right)}{n \cdot K \cdot T}\right] - 1\right\} \\ - I_{sh}\left[1 + \alpha\left(1 - \frac{V + I \cdot R_s}{V_{br}}\right)\right], \end{aligned} \tag{6}$$

where V_{br} (V) is the junction breakdown voltage.

In Simulink, we build submodels for every equation and then encapsulate them together to a whole module/unit (to distinguish the theoretical modules from real PV modules, we use "unit" to represent the encapsulated equations (1)–(5) in Simulink). As shown in Figure 3, the exemplar model for the half-cell module consists of six units, which corresponds to the number of the module's substrings (Figure 1(b)). Each unit is composed of 20 series halved cells and is independent of each other as the input irradiance and temperature can be set up separately. Three bypass diodes and one series diode are also introduced to simulate the electrical interconnection of cells in a PV module. Similarly, the model for the full-cell module consists of three units (half of that of the half-cell model), three bypass diodes and one series diode. Each unit is composed of 20 series full cells.

To simulate the edge soiling, we can change the irradiance proportionally to the shaded area while keeping the temperature at 25°C to draw standard characteristic curves.

Assuming that the incident irradiance on the shaded area (A_s) is 0, the relation between I_{ph} and A_s can be expressed as follows:

$$I_{ph} = \left(1 - \frac{A_s}{A}\right) I_{ph0}, \tag{7}$$

where A is the efficient light absorption area of a cell and I_{ph0} is the unshaded photocurrent at 25°C.

According to equation (1), we can also build the relation between I_{ph} and input irradiance G_i as follows:

$$I_{ph} = \frac{G_i}{G_0} I_{ph0}, \tag{8}$$

where G_0 represents the AM1.5 reference solar spectra, namely, $1000\,W{\cdot}m^{-1}$. Hence, the relation between G_i and A_s can be formulated as follows:

$$G_i = \left(1 - \frac{A_s}{A}\right) G_0, \tag{9}$$

which means G_i is the remaining irradiance received by the shaded cells.

Indeed, it is important to acknowledge that the simulated model used in our study involves significant simplifications, particularly in making the irradiation homogeneous for cells within one substring. In addition, we neglect the current mismatch within substrings by considering them as units. Specifically, when shaded cells in a substring suppress other cells' currents, it can lead to the occurrence of hotspots. However, if all cells within the substring are equally shaded, no hotspot will occur, and the characteristic curves for both cases should be identical (provided they are measured under

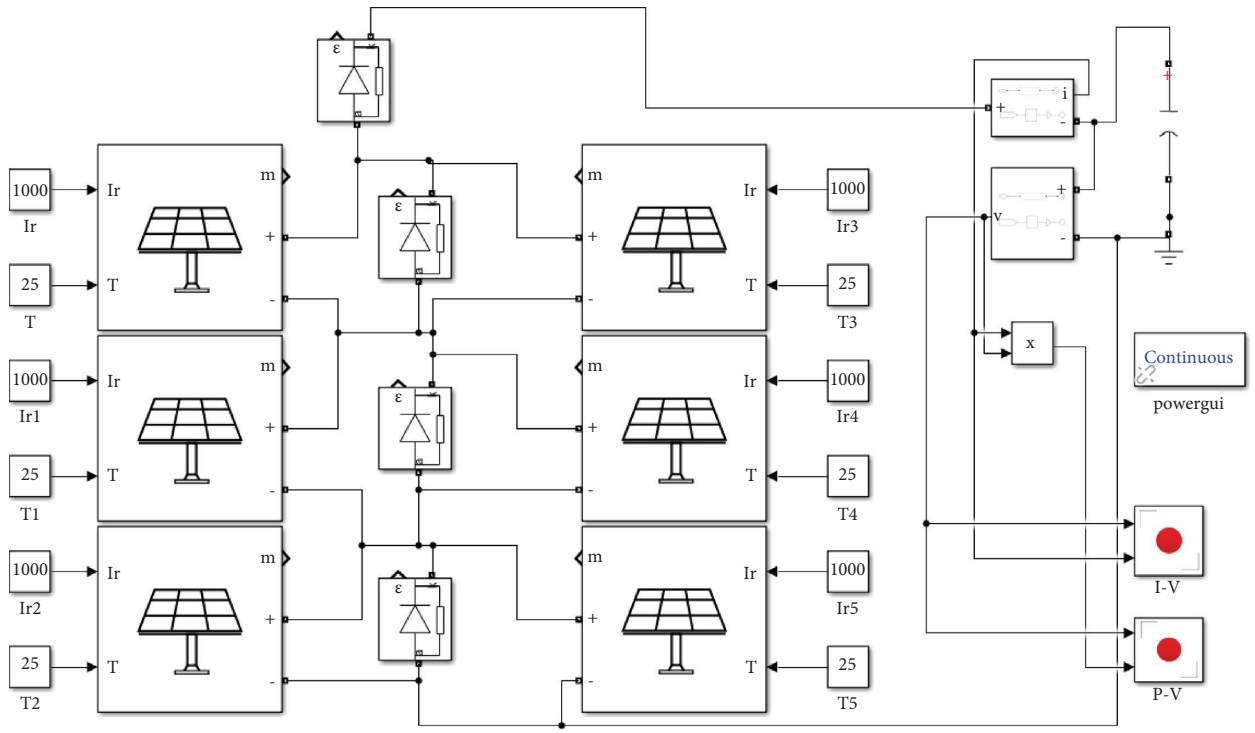

Figure 3: Simulation model by Simulink for the half-cell module. The half-cell module is composed of six units. The first and second three units are connected in series, respectively and then connected in parallel with three bypass diodes. The module is also connected to a series diode, a capacitor, voltmeter, an ammeter, and other measuring units. The small boxes with an arrow pointing to the unit are the input parameters, including irradiance and temperature.

the same temperature). This theoretical simplification is appropriate for studying the effects of edge soiling as discussed in our work and is applicable to most practical scenarios as well.

The standard testing conditions (STC) include ambient temperature (25°C), solar irradiance (ASTM G173-03 reference spectra [24]), and wind speed (0 $m \cdot s^{-1}$). In this work, the PASAN HighLIGHT system (Figure 4) by Meyer Burger is introduced to obtain characteristics and electrical parameters under STC.

As the light source, the lightbox has two lamps with shading sheets and spectral filters. The shading sheets ensure the light is evenly illuminated on the PV modules. The spectral filters can simulate the AM1.5 solar spectra. The generator contains capacitors which are used to adjust the light intensity on the surface of the PV module.

The monitoring battery is connected to the generator at one end and the electronic load at the other. On the one hand, the monitoring battery monitors the irradiance of the module surface, as well as the ambient temperature. Then, it feeds the temperature data back to the electronic load which can issue instructions to adjust the capacitor voltage. On the other hand, the monitoring battery adjusts the target value of the light intensity. Under the combined efforts, the light intensity and the temperature are controlled to strictly meet the standard requirements.

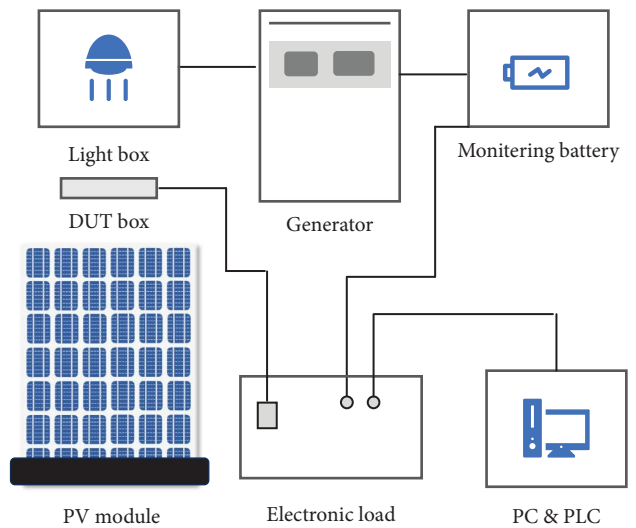

Figure 4: Schematic of the experimental setup. The system is mainly composed of a ministering battery, a lightbox, a generator, an electronic load, and the computer. There is a DUT box between the PV module and the electronic load. A programmable logic controller (PLC) is used to control the system components to maintain the testing conditions. We change the incident irradiation for a certain unit to simulate shading conditions in the simulation model while using opaque covers to shade a certain percentage of cells in the experiment.

There are four distinct soiling patterns corresponding to the full-cell and half-cell modules in both landscape and portrait orientations. In our simulation, we systematically vary the irradiance of individual units within the module. For modules in the landscape orientation, the irradiance of each unit is successively reduced to 1000, 875, 750, 500, 250, and 0 $W{\cdot}m^{-2}$, respectively. Simultaneously, in the experimental setup, we shade a row of cells at different percentages, ranging from 0% (no shading) to 100% (full shading), as depicted in Figures 5(a) and 5(b). Similarly, for modules in the portrait orientation, we reduce the irradiance of three units consecutively to the same values mentioned above (1000, 875, 750, 500, 250, and 0 $W{\cdot}m^{-2}$) through simulation. Correspondingly, in the experimental setup, we shade an entire row of cells at varying percentages, ranging from 0% to 100%, as shown in Figures 5(c) and 5(d).

3. Results and Discussion

Solution to shading effects has always been a heated topic for PV system, while most of the previous work concentrated on the level of PV arrays by reconfiguration. Comprehensive theoretical and experimental studies have been reported on different PV array configurations [25–29]. Limited research has studied on scale of PV modules [30–32]. For instance, Jiadong Qian et al. studied the hotspot effect of half-cell modules using parallel connected cell substrings in comparison with conventional full-cell modules according to the evaluation of the maximum temperature [33]. Compared with previous works, we focus on soiling effects and show a significant impact of mounting orientation and cell interconnection on module performance.

In the landscape orientation, both full-cell and half-cell modules exhibit similar resistance to edge soiling, as shown in Figure 6(a). The characteristics of the modules directly reflect the shading effects, which can be analyzed from a circuit perspective. As the shading ratio increases, the module's short-circuit current remains constant, while the open-circuit voltage experiences a slight decrease. The *I-V* characteristic of the module follows a step-like curve due to the activation of bypass diodes, and the *P-V* characteristic displays two maximum power points (MPPs). When the I-V characteristic follows a step-like curve and the P-V characteristic features multiple MPPs, it indicates that the substrings within the module are shaded to varying degrees. Conversely, if the substrings are uniformly shaded, the short-circuit current will decrease to, the short-circuit current will decline to $I_{sc} = (1 - A_s/A) \cdot I_{sc0}$ and the *P-V* characteristic will have only one MPP.

If we neglect the voltage of bypass diodes, the output current is approximately equal to the nominal short-circuit current, I_{sc0} (~10A) when the voltage climbs from 0 to 20V; and the steady current illustrates the shunt function of bypass diodes. When the voltage continues to increase, the current begins to decline rapidly to $I = (1 - A_s/A) \cdot I_{sc0}$, which means the substring of the shaded cells begins to contribute output power and add its voltage to the module; and the current no longer goes through the bypass diode of the affected substring. As shown by the blue line (legend "100%") in Figure 6(a), the first MPP is approximately equal to 2/3 P_{max} and the output current and power falls to zero at 2/3 V_{oc}. This observation allows us to assume that the first MPP is primarily determined by the other unshaded substrings, and the shaded substring has minimal impact on this MPP. However, as the shading ratio increases from 0 to 100%, the second MPP gradually declines to 0, indicating the significant influence of the shaded substring on the overall module performance.

For the full-cell modules in the portrait orientation (Figures 7(a) and 7(c)), we observe that the open-circuit voltage experiences a slight decrease, while the short-circuit current directly declines to $I_{sc} = (1 - A_s/A) \cdot I_{sc0}$ directly with the increase of the shading radio. The *P-V* characteristic exhibits only one maximum power point (MPP), indicating that the bypass diodes are reverse biased. This outcome arises because the edge soiling simultaneously affects three substrings (Figure 5(c)). Moreover, there is no current mismatch in the module circuit since the currents in each substring are identical, owing to consistent shading ratios for every substring. Analyzing the *P-V* characteristic curve further reveals that the trend of the MPP with output voltage closely resembles the I_{sc}, which is proportionate to $(1 - A_s/A)$. When the shading ratio reaches 100%, the module output falls to zero. According to Figures 6(a) and 6(c), when the full-cell modules are mounted with landscape orientation, the MPP reaches 2/3 P_{max} even though the bottom row is completely shaded; however, multiple MPPs are still a problem waiting to be addressed by other tracking technologies. When mounted with portrait orientation, the MPP vanishes when the bottom row is completely shaded; and it decreases more quickly with the increase of shading ratio (Figures 7(a) and 7(c)). The results make the landscape orientation more advantageous for the full-cell modules.

For the half-cell modules in the portrait orientation (Figures 7(b) and 7(d)), the short-circuit current declines to $I_{sc} = (1 - 0.5 \cdot A_s/A) \cdot I_{sc0}$ with the increase of the shading radio. Interestingly, the MPP still reaches 1/2 of P_{max} even when the shading ratio is 100% (for the full-cell module, MPP is 0). In other words, with portrait mounting orientation, the half-cell module shows better performance than the full-cell module against edge soiling. The advantage stems from the fact that the half-cell module has twice as many independent substrings as the full-cell module. When some substrings are shaded, the others continue to normally work thanks to the bypass diodes and parallel interconnection. Consequently, the impact of shading is proportional to the ratio of shaded substrings over the module. It is noteworthy that the landscape orientation is not always superior to the portrait orientation for half-cell modules, unlike the case with full-cell modules. Instead, the performance in the portrait orientation surpasses that in the landscape orientation when the shading ratio is less than 50% (Figures 6(b), 6(c), 7(b), and 7(c)).

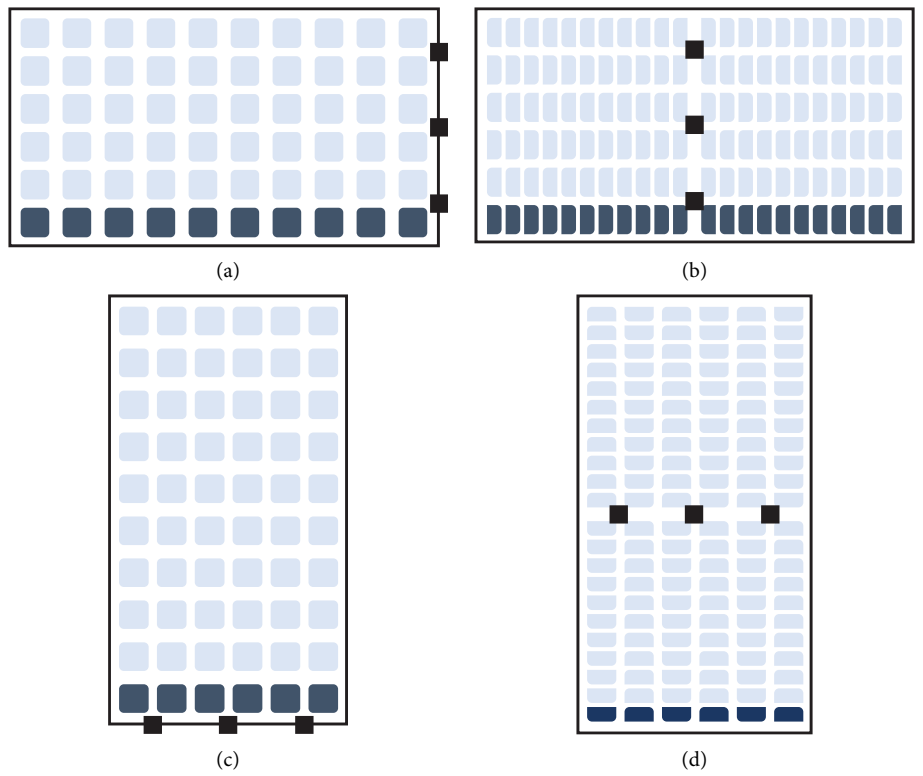

Figure 5: Schematics of edge soiling. The deep blue squares represent the shaded cells while the light blue squares represent the unshaded ones. (a, b) Edge soiling for the full-cell and half-cell modules in the landscape orientation, respectively. (c, d) Edge soiling for the full-cell and half-cell modules in the portrait orientation, respectively.

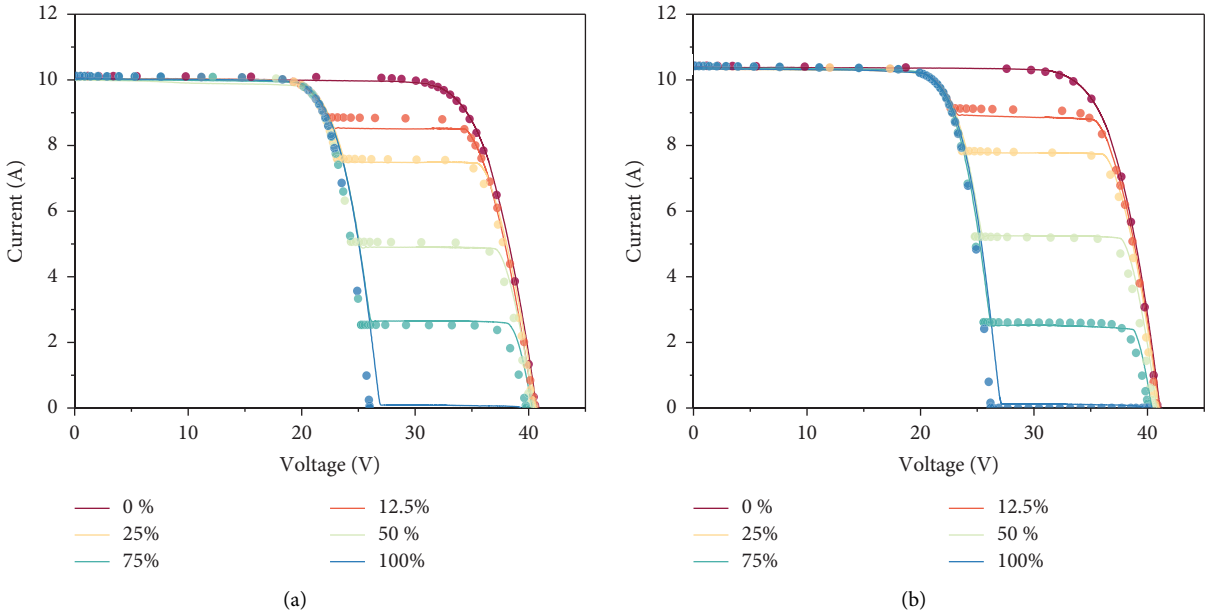

Figure 6: Continued.

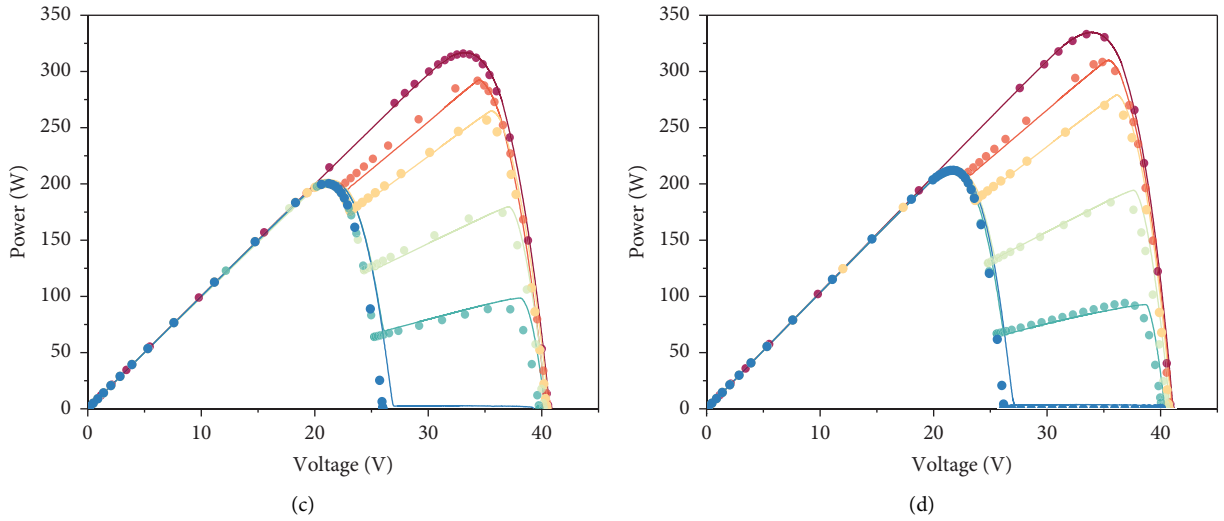

Figure 6: Edge soiling effects on the landscape-mounted modules. (a, c) Characteristic *I-V* and *P-V* curves for the full-cell modules under edge soiling. (b, d) Characteristic *I-V* and *P-V* curves for the half-cell modules under edge soiling.

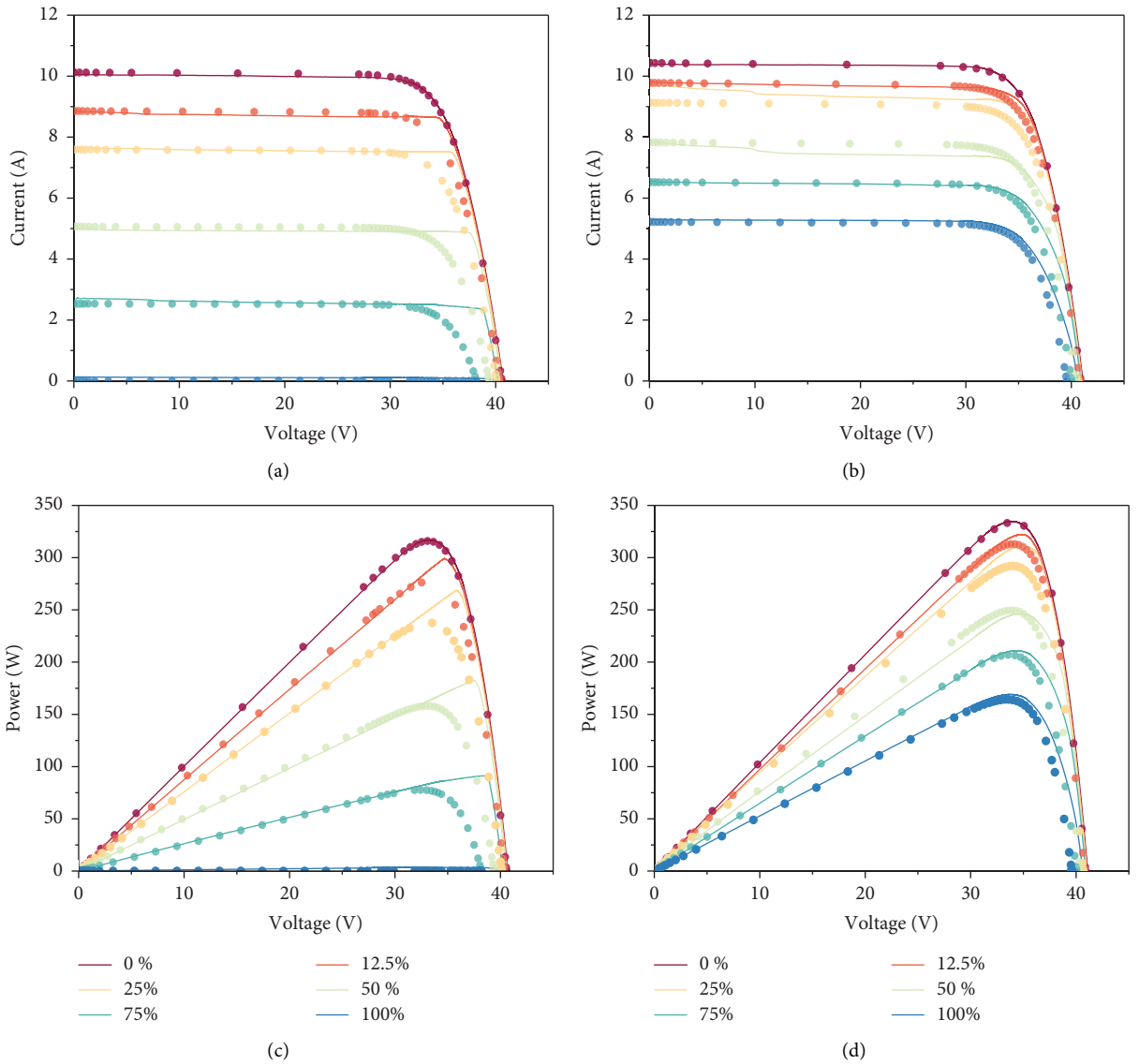

Figure 7: Edge soiling effects on the portrait-mounted modules. (a, c) Characteristic *I-V* and *P-V* curves for the full-cell modules under edge soiling. (b, d) Characteristic *I-V* and *P-V* curves for the half-cell modules under edge soiling.

Table 2: Comparative summary of module mounting orientations.

Edge shading ratio (%)	Full-cell modules	Half-cell modules
Below 50%	Landscape	Portrait
50% and above	Landscape	Landscape

4. Conclusion

This work provides a comprehensive investigation into the edge soiling effects on both full-cell and half-cell modules. The simulation procedure involves the development of a practical and straightforward model for both PV modules using Simulink. In the experimental setup, we utilize the PASAN HighLIGHT system to achieve the standard testing condition and measure the shaded characteristics of both PV modules in both landscape and portrait mounting orientations. Both the simulated and experimental parts are validated and replicable. By uncovering the distinctions between full-cell and half-cell modules in different mounting orientations, this research offers valuable insights for designing distributed PV systems to maximize efficiency and performance under varying shading conditions.

Notably, while the half-cell modules do not demonstrate superiority over the full-cell modules in the landscape orientation, they exhibit better resistance to edge soiling when mounted in the portrait orientation. The extent of edge soiling's influence is directly proportional to the ratio of shaded substrings within a module. For full-cell modules, the landscape mounting orientation is preferred when considering edge soiling, as the MPP reduces to 0 in the portrait orientation when the bottom row is entirely shaded. In contrast, for half-cell modules, the MPP with portrait orientation outperforms the landscape orientation when the shading ratio is less than 50% (Table 2). Therefore, other factors such as available areas and supporting structures should be considered during practical installation to decide the optimal mounting orientations for half-cell modules. These findings contribute to the advancement of PV technology and the promotion of sustainable and reliable renewable energy systems for practical applications. Although this work only discussed commercial PV modules, more sophisticated interconnections of cells can be designed to further improve the resilience of edge soiling. Besides, other parameters such as local heating and irregular shading can be included in future research.

Data Availability

All the data used to support the findings of this study are available from the first author upon request.

Conflicts of Interest

The authors declare that they have no conflicts of interest.

Acknowledgments

We would like to express our gratitude to Jing Huang, Jia Liao, and Bowen Lü for their assistance in the experimental work. Sincere thanks to Associate Professor Genxiang Zhong Associate Professor Yaofeng Zhang of the Photovoltaic Power Generation System Control and Optimization Engineering Laboratory of Hunan Province for providing the experimental conditions and training. This work was funded by Innovative Research Team of Guangdong University of Science and Technology (Grant no. GKY-2022CQTD-1).

References

[1] J. M. Carrasco, L. G. Franquelo, J. T. Bialasiewicz et al., "Power-electronic systems for the grid integration of renewable energy sources: a survey," *IEEE Transactions on Industrial Electronics*, vol. 53, no. 4, pp. 1002–1016, 2006.

[2] S. Gorjian, H. Ebadi, L. D. Jathar, and L. Savoldi, "Chapter 1-solar energy for sustainable food and agriculture: developments, barriers, and policies," in *Solar Energy Advancements in Agriculture and Food Production Systems*, S. Gorjian and P. E. Campana, Eds., pp. 1–28, Academic Press, Cambridge, MA, USA, 2022.

[3] G. Luo, C. Long, X. Wei, and W. Tang, "Financing risks involved in distributed PV power generation in China and analysis of countermeasures," *Renewable and Sustainable Energy Reviews*, vol. 63, pp. 93–101, 2016.

[4] S. Sanyal, A. Tewary, R. Kumar et al., "Performance and degradation analysis of high-efficiency SPV modules under composite climatic condition," in *Proceedings of the 7th International Conference on Advances in Energy Research*, M. Bose and A. Modi, Eds., pp. 869–878, Springer Proceedings in Energy; Springer, Singapore, 2021.

[5] K. Ilse, L. Micheli, B. W. Figgis et al., "Techno-economic assessment of soiling losses and mitigation strategies for solar power generation," *Joule*, vol. 3, no. 10, pp. 2303–2321, 2019.

[6] H. Hanifi, M. Z. Khan, B. Jaeckel et al., "Optimum PV module interconnection layout and mounting orientation to reduce inhomogeneous soiling losses in desert environments," *Solar Energy*, vol. 203, pp. 267–274, 2020.

[7] L. D. Jathar, S. Ganesan, K. Shahapurkar et al., "Effect of various factors and diverse approaches to enhance the performance of solar stills: a comprehensive review," *Journal of Thermal Analysis and Calorimetry*, vol. 147, no. 7, pp. 4491–4522, 2022.

[8] L. D. Jathar, S. Ganesan, U. Awasarmol et al., "Comprehensive review of environmental factors influencing the performance of photovoltaic panels: concern over emissions at various phases throughout the lifecycle," *Environmental Pollution*, vol. 326, Article ID 121474, 2023.

[9] T. M. Yunus Khan, M. E. M. Soudagar, M. Kanchan et al., "Optimum location and influence of tilt angle on performance of solar PV panels," *Journal of Thermal Analysis and Calorimetry*, vol. 141, no. 1, pp. 511–532, 2020.

[10] K. Chandrakant Nikam, L. Jathar, S. D. Shelare et al., "Parametric analysis and optimization of 660 MW supercritical power plant," *Energy*, vol. 280, Article ID 128165, 2023.

[11] N. Agrawal, B. Bora, and A. Kapoor, "Experimental investigations of fault tolerance due to shading in photovoltaic modules with different interconnected solar cell networks," *Solar Energy*, vol. 211, pp. 1239–1254, 2020.

[12] E. Diaz-Dorado, J. Cidras, and C. Carrillo, "Discrete I-V model for partially shaded PV-arrays," *Solar Energy*, vol. 103, pp. 96–107, 2014.

[13] M. B. Ogaard, H. N. Riise, H. Haug, S. Sartori, and J. H. Selj, "Photovoltaic system monitoring for high latitude locations," *Solar Energy*, vol. 207, pp. 1045–1054, 2020.

[14] K. Chandrasekaran, S. Sankar, and K. Banumalar, "Partial shading detection for PV arrays in a maximum power tracking system using the sine-cosine algorithm," *Energy for Sustainable Development*, vol. 55, pp. 105–121, 2020.

[15] E. Piccoli, A. Dama, A. Dolara, and S. Leva, "Experimental validation of a model for PV systems under partial shading for building integrated applications," *Solar Energy*, vol. 183, pp. 356–370, 2019.

[16] R. Witteck, M. Siebert, S. Blankemeyer, H. Schulte-Huxel, and M. Köntges, "Three bypass diodes architecture at the limit," *IEEE Journal of Photovoltaics*, vol. 10, no. 6, pp. 1828–1838, 2020.

[17] K. Osmani, A. Haddad, H. Jaber, T. Lemenand, B. Castanier, and M. Ramadan, "Mitigating the effects of partial shading on PV system's performance through PV array reconfiguration: a review," *Thermal Science and Engineering Progress*, vol. 31, Article ID 101280, 2022.

[18] L. D. Jathar, S. Ganesan, and S. Gorjian, "An experimental and statistical investigation of concave-type stepped solar still with diverse climatic parameters," *Cleaner Engineering and Technology*, vol. 4, Article ID 100137, 2021.

[19] J. Mueller, D. Hinken, S. Blankemeyer et al., "Resistive power loss analysis of PV modules made from halved 15.6 x 15.6 Cm(2) silicon PERC solar cells with efficiencies up to 20.0%," *IEEE Journal of Photovoltaics*, vol. 5, no. 1, pp. 189–194, 2015.

[20] S. Guo, J. P. Singh, I. M. Peters, A. G. Aberle, and T. M. Walsh, "A quantitative analysis of photovoltaic modules using halved cells," *International Journal of Photoenergy*, vol. 2013, Article ID 739374, 8 pages, 2013.

[21] Y.-J. Wang and P.-C. Hsu, "An investigation on partial shading of PV modules with different connection configurations of PV cells," *Energy*, vol. 36, no. 5, pp. 3069–3078, 2011.

[22] H. Patel and V. Agarwal, "MATLAB-based modeling to study the effects of partial shading on PV array characteristics," *IEEE Transactions on Energy Conversion*, vol. 23, no. 1, pp. 302–310, 2008.

[23] J. W. Bishop, "Computer simulation of the effects of electrical mismatches in photovoltaic cell interconnection circuits," *Solar Cells*, vol. 25, no. 1, pp. 73–89, 1988.

[24] NREL, "Reference air mass 1.5 spectra," 2023, https://www.nrel.gov/grid/solar-resource/spectra-am1.5.html.

[25] F. Belhachat and C. Larbes, "Modeling, analysis and comparison of solar photovoltaic array configurations under partial shading conditions," *Solar Energy*, vol. 120, pp. 399–418, 2015.

[26] G. Sai Krishna and T. Moger, "Improved SuDoKu reconfiguration technique for total-cross-tied PV array to enhance maximum power under partial shading conditions," *Renewable and Sustainable Energy Reviews*, vol. 109, pp. 333–348, 2019.

[27] I. Nasiruddin, S. Khatoon, M. F. Jalil, and R. C. Bansal, "Shade diffusion of partial shaded PV array by using odd-even structure," *Solar Energy*, vol. 181, pp. 519–529, 2019.

[28] M. Balato, L. Costanzo, and M. Vitelli, "Series-parallel PV array Re-configuration: maximization of the extraction of energy and much more," *Applied Energy*, vol. 159, pp. 145–160, 2015.

[29] S. Mohammadnejad, A. Khalafi, and S. M. Ahmadi, "Mathematical analysis of total-cross-tied photovoltaic array under partial shading condition and its comparison with other configurations," *Solar Energy*, vol. 133, pp. 501–511, 2016.

[30] M. C. A. García, W. Herrmann, W. Böhmer, and B. Proisy, "Thermal and electrical effects caused by outdoor hot-spot testing in associations of photovoltaic cells," *Progress in Photovoltaics: Research and Applications*, vol. 11, no. 5, pp. 293–307, 2003.

[31] M. Danner and K. Bucher, "Reverse characteristics of commercial silicon solar cells-impact on hot spot temperatures and module integrity," in *Proceedings of the Conference Record of the Twenty Sixth IEEE Photovoltaic Specialists Conference*, pp. 1137–1140, Anaheim, CA, USA, September 1997.

[32] S. Deng, Z. Zhang, C. Ju et al., "Research on hot spot risk for high-efficiency solar module," *Energy Procedia*, vol. 130, pp. 77–86, 2017.

[33] J. Qian, C. E. Clement, M. Ernst, Y. S. Khoo, A. Thomson, and A. Blakers, "Analysis of hotspots in half cell modules undetected by current test standards," *IEEE Journal of Photovoltaics*, vol. 9, no. 3, pp. 842–848, 2019.